PCCP

Two-photon dissociation dynamics of the mercapto radical

Journal:	*Physical Chemistry Chemical Physics*
Manuscript ID	CP-ART-09-2022-004116.R1
Article Type:	Paper
Date Submitted by the Author:	12-Oct-2022

Complete List of Authors:	Qin, Yuan; University of California Riverside Zheng, Xianfeng; Anhui Normal University Song, Yu; University of California at Riverside, Department of Chemistry Sun, Ge; University of California at Riverside, Department of Chemistry Zhang, Jingsong; University of California at Riverside, Department of Chemistry

Two-photon dissociation dynamics of the mercapto radical

Yuan Qin, Xianfeng Zheng[a], Yu Song[b], Ge Sun[c], and Jingsong Zhang*

Department of Chemistry

University of California at Riverside

Riverside, California 92521

U.S.A.

Abstract

Two-photon dissociation dynamics of the SH/SD radicals are investigated using the high-*n* Rydberg atom time-of-flight (HRTOF) technique. The H/D(^{2}S) + S(^{1}D) and H/D(^{2}S) + S(^{1}S) products are observed in the dissociation of the SH/SD radicals on the $2^2\Pi$ and $B^2\Sigma^+$ repulsive states, from sequential two-photon excitation via the $A^2\Sigma^+$ ($v' = 0$, $J' = 0.5$-2.5) state. The angular distributions of both H/D(^{2}S) + S(^{1}D) and H/D(^{2}S) + S(^{1}S) product channels are anisotropic. The anisotropy parameter (β) of the H(^{2}S) + S(^{1}D) products is ~ −0.8 ± 0.1 (−0.9 ± 0.05 for SD), and that of the H(^{2}S) + S(^{1}S) products is ~ 1.3 ± 0.3 (1.2 for SD). The anisotropic angular distributions indicate that the SH/SD radicals promptly dissociate on the repulsive $2^2\Pi$ and $B^2\Sigma^+$ potential energy curves (PECs) along with some non-adiabatic crossings, leading to the H/D(^{2}S) + S(^{1}D) and H/D(^{2}S) + S(^{1}S) products, respectively. The bond dissociation energy of the ground-state $X^2\Pi_{3/2}$ SH/SD to the ground-state H/D(^{2}S) + S(^{3}P$_2$) products is measured to be D_0(S−H) = 29253 ± 20 cm^{-1} and D_0(S−D) = 29650 ± 20 cm^{-1}, respectively. The dissociation energy of the $A^2\Sigma^+$ state SH/SD to the H/D(^{2}S) + S(^{1}D) products is derived to be D_0[S−H(A)] = 7659 ± 20 cm^{-1} and D_0[S−D(A)] = 7940 ± 20 cm^{-1}.

a. Permanent address: Department of Physics, Anhui Normal University, Wuhu, Anhui 241000, P. R. China.

b. Permanent address: Beijing Academy of Quantum Information Sciences, Beijing, 100193, P. R. China.

c. Permanent address: Dalian Institute of Chemical Physics, Chinese Academy of Sciences, Dalian, Liaoning 116023, P. R. China.

* Corresponding author. E-mail: jingsong.zhang@ucr.edu. Fax: 1-951-827-4713. Also at the Air Pollution Research Center, University of California, Riverside, CA 92521, USA.

Introduction

The mercapto radical (SH) is a prototype open-shell diatomic system. It is also of importance in the atmospheric chemistry of sulfur, fossil fuel combustion, and astrochemistry. When excited by ultraviolet light, the SH/SD radical can readily produce highly reactive fragments such as $S(^3P)$ and $S(^1D)$. The photodissociation processes involve multiple potential energy curves (PECs) and non-adiabatic interactions. With the relatively simple electronic structure, the photolysis of the SH/SD radical can provide benchmarks for theoretical studies of open-shell species.

The electronic states and spectroscopy of SH/SD have been extensively studied both theoretically[1-8] and experimentally.[9-17] Figure 1 shows the PECs of the electronic states of SH. The ground electronic state, $X^2\Pi$, correlates asymptotically to the $H(^2S) + S(^3P_J)$ products. The first excited state, $A^2\Sigma^+$, correlates to the excited state products $H(^2S) + S(^1D)$ and is crossed by three repulsive states $^4\Sigma^-$, $^2\Sigma^-$, and $^4\Pi$, which correlate with the ground-state products $H(^2S) + S(^3P_J)$. Two other high-energy states, $^2\Delta$ and $2^2\Pi$, correlate asymptotically to $H(^2S) + S(^1D)$, whereas

another state, $B^2\Sigma^+$, crosses with $2^2\Pi$ and correlates to $H(^2S) + S(^1S)$. The $2^4\Sigma^-$ and $2^2\Sigma^-$ states at higher energy are the lowest Rydberg states of SH and both are crossed with $^2\Delta$, $^4\Pi$, $2^2\Pi$, and $B^2\Sigma^+$. As the $A^2\Sigma^+$ state can undergo predissociation via spin-orbit couplings with the three repulsive states ($^4\Sigma^-$, $^2\Sigma^-$, and $^4\Pi$), the spectroscopy of the $A^2\Sigma^+ \leftarrow X^2\Pi$ band system,[5, 9-13, 17-28] as well as the predissociation dynamics, has been of interest in both theoretical[5, 6, 17, 29, 30] and experimental studies.[11-13, 23-26] The lifetimes of the different vibrational levels of the $A^2\Sigma^+$ state are affected by predissociation. The experimentally measured lifetimes is $\tau \approx$ 3 ns for SH $v' = 0$,[11, 12, 23] ~ 200 ns for SD $v' = 0$,[12, 13, 17, 24] and ~ 35ps for SD $v' = 1$.[17] As the vibrational level increases, they are closer to the crossings of the $A^2\Sigma^+$ state and the three repulsive states, and thus the lifetime decreases to a few picoseconds for both SH and SD.[17] The predissociation of the $A^2\Sigma^+$ state at lower vibrational levels ($v' = 0$-1 of SH and $v' = 0$-2 of SD) occur mainly via the $^4\Sigma^-$ state, and all the three repulsive states ($^4\Sigma^-$, $^2\Sigma^-$, and $^4\Pi$) are involved in the predissociation of the higher vibrational levels. The experimental fine-structure branching fractions of the $S(^3P_{J=0,1,2})$ products from the predissociation of SH/SD at $A^2\Sigma^+$ $v' = 0$-2 suggest that predissociation dynamics follows coupling from the $A^2\Sigma^+$ state to the $^4\Sigma^-_{1/2}$ potential along with nonadiabatic interactions at large internuclear distance.[26] The product angular distributions from the predissociation of SH/SD at different rovibrational levels of the $A^2\Sigma^+$ state were acquired, and the measured anisotropy parameter β shows strong dependence on the different rotational transitions.[26] In addition, photodissociation of SH/SD ($X^2\Pi$, $v'' = 2$-7) via the repulsive wall of the $A^2\Sigma^+$ state has been observed, and the $S(^1D)$ products were detected.[31]

In the vacuum ultraviolet (VUV) region, several Rydberg states of SH have been observed.[32-35] Morrow obtained the one-photon VUV absorption spectrum of SH/SD between 123-200 nm,[32] and seven Rydberg states were identified: $B^2\Sigma^-$ $[(2\pi)^2 4s]$ (which is the first doublet

Rydberg state, labeled as $2^2\Sigma^-$ in later literature),[2, 3] $C^2\Sigma^-$ $[(2\pi)^2 4P_\sigma]$,[2, 3, 33] $E^2\Sigma^-$ $[(2\pi)^2 3D_\sigma]$,[2] and D, F, G, and $H^2\Delta$ $[(2\pi)^2 nd_\sigma$, n = 3-6][2] states that converge to the $X^3\Sigma^-$ ground ionic state of SH. Later on, 2 + 1 resonance enhanced multiphoton ionization (REMPI) studies observed another Rydberg state with the $X^3\Sigma^-$ ionic core, $^2\Pi$ $[(2\pi)^2 4P_\pi]$,[33] and fourteen more Rydberg states that converge upon the excited ionic states $a^1\Delta$ and $b^1\Sigma^+$ of SH^+.[34, 35] In general, these Rydberg states are bound in the Franck-Condon (FC) region of SH and are correlated with higher excited states of the S atom product. The experimental and theoretical investigations on the photodissociation of SH/SD via the higher repulsive electronic states remain limited.[36-42] The secondary photodissociation of SH from UV photolysis of H_2S at 218.1 nm was examined by Ashfold and coworkers;[38, 39] the $S(^3P_J)$ fine-structure state distribution measured by REMPI and kinetic energy distribution of the H atom product suggested the involvement of the perpendicular SH $^2\Sigma^- \leftarrow X^2\Pi$ transition. Continetti et al.[36] and Hsu et al.[37] studied secondary photolysis of SH in 193 nm photodissociation of H_2S. Although their observed $S(^3P)$:$S(^1D)$ product branching ratios were different (3:1 by Continetti et al.[36] and 6.7:1 by Hsu et al.[37]), both concluded that $S(^3P)$ and $S(^1D)$ were produced from direct photodissociation of SH at 193 nm via the repulsive states $^2\Sigma^-$ and $^2\Delta$. Later, the UV photodissociation of jet-cooled SH radical was studied in the region of 216-232 nm (and 220-244 nm for SD) by Zhang and co-workers using the high-*n* Rydberg atom time-of-flight (HRTOF) technique.[40, 42] The anisotropy β parameter of the H/D-atom product was ~ -1, consistent with the perpendicular $^2\Sigma^- \leftarrow X^2\Pi$ transition and a prompt dissociation. The $S(^3P_J)$ spin-orbit branching fraction was $S(^3P_2):S(^3P_1):S(^3P_0)$ = 0.51:0.36:0.13 (0.51:0.37:0.12 for SD), approaching that in a sudden limit dissociation on the repulsive $^2\Sigma^-$ state. The VUV photodissociation of SH at 121.6 nm was investigated by Zhang and coworkers,[41] and the $S(^3P)$, $S(^1D)$ and $S(^1S)$ products were observed with a ratio of 0.07:0.82:0.11. It is believed that excitation to the $2^2\Pi$ state

contributes most to the photodissociation of SH at 121.6 nm while the $^2\Delta$ state could also contribute;[41] both states correlate to the S(^{1}D) product. The S(^{1}S) product should result from the $B^2\Sigma^+$ state. The spin-orbit branching fraction of the minor S(^3P_J) products is S($^3P_2$):S($^3P_1$):S($^3P_0$) = 0.28:0.54:0.18, significantly different from that via the $^2\Sigma^-$ state in the UV region. This S(^3P_J) ratio is close to that of the sudden limit of the $^4\Pi$ state, which could be coupled via spin-orbit interactions with the $^2\Delta$ state or the $2^2\Pi$ state starting from the FC region.

In this work, we report an investigation on the H/D(^{2}S) + S(^{1}D) and H/D(^{2}S) + S(^{1}S) product channels in the photodissociation of the SH/SD radical from higher exited electronic states, following two-photon excitation via the intermediate $A^2\Sigma^+$ state. The H/D(^{2}S) + S(^{1}D) and H/D(^{2}S) + S(^{1}S) product channels are both directly observed in the H/D-atom product time-of-flight (TOF) spectra, and the product anisotropy parameters are measured. The nature of the involved electronic excited states and the dissociation dynamics of SH/SD are characterized. Accurate SH and SD bond dissociation energies D_0(S−H) and D_0(S−D) of the ground state and dissociation energy of the $A^2\Sigma^+$ state D_0[S−H(A)] and D_0[S−D(A)] are also determined.

Experimental

The HRTOF technique was used in this study and the detailed description of the experimental setup has been reported in previous publications.[40, 42-44] A mixture of ~ 6% H_2S (≥ 99.5%, Aldrich) or ~ 9% D_2S (≥ 98%, Cambridge Isotope Laboratories) precursor in Ar (at a total pressure of ~ 1.2 atm) was expanded through a pulsed nozzle. In front of the nozzle the SH or SD molecular beam was generated by photolyzing the precursors with a 193 nm radiation from an ArF excimer laser. The SH/SD radicals produced from photolysis were subsequently cooled by

supersonic expansion and collimated by a skimmer downstream into the high-vacuum main chamber. The effective rotational temperature of the SH radicals in the beam was estimated to be ~ 45 K (~ 25 K for the SD radicals), based on the relative signal intensities from several initial rotational levels of the $X^2\Pi$ ground state. Crossed with a tunable, linearly polarized UV laser radiation (around 324 nm for SH and 323 nm for SD, 5-8 mJ/pulse, slightly focused with a 100-cm focal length lens, linewidth ~ 0.3 cm^{-1}), the SH/SD radicals were photodissociated in the region of intersection. The photolysis laser wavelength was tuned to the resonant excitations of the previously studied SH and SD transitions $A^2\Sigma^+$ (v' = 0, J' = 0.5-2.5, F_1) ← $X^2\Pi$ (v'' = 0, J'' = 1.5, F_1), i.e., $P_1(1.5)$, $Q_1(1.5)$, and $R_1(1.5)$, at 30832.68, 30849.42, and 30882.71 cm^{-1} for SH; and 30948.24, 30957.29, and 30974.27 cm^{-1} for SD, respectively.[9] A wavemeter (Burleigh WA-4500) was used to monitor the absolute photolysis wavelength. The linear polarization of the photolysis radiation can be rotated by a Fresnel-Rhomb achromatic λ/2 plate for product angular distribution measurements. After the photodissociation, the H/D-atom products were pumped by two-color resonant excitation (121.6 nm + 366.2 nm), i.e., from 1^2S to 2^2P state via the Lyman-α transition and then to a metastable high-n Rydberg state. A small portion of the Rydberg H/D atoms drifted with nascent velocities toward a microchannel plate (MCP) detector, and were then field ionized in front of the detector and detected. The flight length was calibrated to be 37.30 cm by the photodissociation of HBr, with its well-known bond dissociation energy and the spin-orbit splitting energy between the Br ($^2P_{3/2}$) and Br ($^2P_{1/2}$) products. The flight distance was further refined using the energetics of the two-photon photodissociation products H(^2S) + S(^1D) and H(^2S) + S(^1S) and the one-photon photodissociation product H(^2S) + S(^3P), which is discussed later. The H/D-atom TOF spectra were typically accumulated with ~ 10-40 k laser firings.

Results

Figure 2 shows the H-atom TOF spectra on and off the $P_1(1.5)$ transition of the SH (0,0) band, i.e. $A^2\Sigma^+$ ($v' = 0$, $N' = 0$, $J' = 0.5$, F_1) ← $X^2\Pi$ ($v'' = 0$, $N'' = 1$, $J'' = 1.5$, F_1), with the photolysis radiation polarization perpendicular (⊥, θ = 90°) and parallel (∥, θ = 0°) to the TOF path, respectively. In addition to the three strong peaks at the flight time of 60-80 μs, there are two sharp peaks locating at ~ 16 and 24 μs in the H-atom TOF spectra. As displayed in Figure 2, these peaks disappear when the photolysis wavelength is off the transition resonance (slightly shifted by ~ 6 cm^{-1}), except for several minor peaks at ~ 23 and 26-27 μs. The H-atom peaks at 60-80 μs show a linear dependence on the photolysis laser power, while a nonlinear relationship between the intensities of the peaks around 16 and 24 μs and the laser power suggests multi-photon processes. The signals around 16 and 24 μs present strong dependences on the polarization of the photolysis radiation. The peak near 16 μs has a much stronger signal at the perpendicular polarization than at the parallel polarization. The intensity for the peak at ~ 24 μs is intense at the parallel polarization and very small/negligible at the perpendicular polarization. Similar observations are found in the H-atom TOF spectra of the SH radical at the photolysis wavelengths on the $Q_1(1.5)$ and $R_1(1.5)$ transition resonances, likewise the signals present at the longer flight time (~ 23 and 35 μs) in the H-atom TOF spectra of the $P_1(1.5)$, $Q_1(1.5)$, and $R_1(1.5)$ transitions of the SD (0,0) band (not shown here). As discussed later, the peaks at 60-80 μs in Figure 2 are assigned to the $H(^2S) + S(^3P_J)$ products due to one-photon dissociation via the SH $A^2\Sigma^+$ state, while the peaks at ~16 and 24 μs are from two-photon dissociation to the $H(^2S) + S(^1D)$ and $H(^2S) + S(^1S)$ products, respectively. When the photolysis wavelengths are off the $P_1(1.5)$, $Q_1(1.5)$ and $R_1(1.5)$ transition resonances, the disappearance of the signals at 60-80 μs confirms the photodissociation via the $A^2\Sigma^+$ state. The disappearance of the peaks at ~ 16 and 24 μs in the off-resonance TOF spectra indicates a

sequential absorption of two photons where the second photon starts sequentially from the $A^2\Sigma^+$ state, rather than a concerted two-photon process. The lifetime of the intermediate state $A^2\Sigma^+$ ($v' = 0$, $J' = 0.5$) of SH is on the order of 3 ns,[11, 12, 28] readily allowing sequential absorption of another photon in the 7-ns excitation laser pulse. The minor peaks at ~ 23 and 26 μs remained in the off-resonance spectra, and they could be attributed to transitions from the vibrationally excited $X^2\Pi$ to the repulsive $^2\Sigma^-$ state: $^2\Sigma^- \leftarrow X^2\Pi$ ($v'' = 4$) and $^2\Sigma^-/A^2\Sigma^+$ ($v' = 7$) $\leftarrow X^2\Pi$ ($v'' = 3$), respectively, leading to the $H(^2S) + S(^3P_J)$ products. Similar analysis of the on and off resonance D-atom TOF spectra from SD also confirms that the sharp peaks at ~ 23 and 35 μs are from the sequential two photon dissociation of SD to the $D(^2S) + S(^1D)$ and $D(^2S) + S(^1S)$ products, respectively, via the $A^2\Sigma^+$ intermediate state. The lifetime of the intermediate state $A^2\Sigma^+$ ($v' = 0$, $J' = 0.5$) of SD is on the order of 200 ns,[12, 13, 24] significantly longer than the 7-ns excitation laser pulse.

The net H/D-atom TOF spectra (after removal of background with the 193-nm radical production laser radiation off) can be directly converted to the H/D + S product center-of-mass (CM) translational energy distributions, $P(E_T)$, using the following equation (using SH as the example):

$$E_T = \left(1 + \frac{m_H}{m_S}\right)E_H + \frac{m_H}{m_S}E_{SH} = \frac{1}{2}m_H\left(1 + \frac{m_H}{m_S}\right)\left(\frac{L}{t_H}\right)^2 + \frac{m_H}{m_S}E_{SH} \quad (1)$$

where E_H and E_{SH} are the laboratory translational energies of the H-atom product and the parent SH radical, L is the length of the TOF path, and t_H is the H-atom flight time. The second term ($\frac{m_H}{m_S}$ E_{SH}) is due to the parent SH radical motion in the molecular beam, which is perpendicular to the TOF path. This term is estimated to be ~ 14 cm^{-1} (~ 29 cm^{-1} for SD), based on the estimated beam velocity of ~ 560 m/s for the SH/Ar gas mixture. Figure 3 presents the angle-dependent $P(E_T,\theta)$ distributions of the H + S products from the photodissociation of the SH radical via the $P_1(1.5)$

transition, at the perpendicular and parallel photolysis polarizations, which are transformed from the TOF spectra in Figure 2. In the $P(E_T,\theta)$ distributions in Figure 3, three peaks in the range of 1000-1600 cm^{-1} (the TOF peaks at 60-80 μs) have comparable intensities at both polarizations, i.e., an isotropic angular distribution. These peaks are identified to be the $H(^2S) + S(^3P_J)$ products from the predissociation of the SH radical via the $A^2\Sigma^+$ ($v' = 0$, $N' = 0$, $J' = 0.5$, F_1) state (the $P_1(1.5)$ transition) following one-photon excitation. Similar observations are found in the $P(E_T,\theta)$ distributions when the photolysis laser tuned to the $Q_1(1.5)$ and $R_1(1.5)$ transitions, i.e. predissociation via the $A^2\Sigma^+$ ($v' = 0$, $N' = 1$ and 2, $J' = 1.5$ and 2.5) states, but with different product angular distributions. In a one-photon dissociation process, the photofragment angular distributions lead to the angle-dependent $P(E_T,\theta)$ distributions, which can be described with the following equation:

$$P(E_T,\theta) = \frac{1}{4\pi}P(E_T)[1 + \beta(E_T)P_2(cos\theta)] \quad (2)$$

where $P(E_T)$ is the angle integrated distribution, β is the anisotropy parameter ($-1 \leq \beta \leq 2$), θ is the angle between the electric vector of the linearly polarized photolysis radiation and the velocity vector of the detected H-atom product (the TOF axis), and $P_2(cos\theta)$ is the second Legendre polynomial.[45] The derived anisotropy parameter of the $H(^2S) + S(^3P_J)$ products for the one-photon dissociation of SH $A^2\Sigma^+$ via the $P_1(1.5)$ transition is ≈ 0.0, while the β value is slightly negative at the $Q_1(1.5)$ transition (~ −0.1) and slightly positive at the $R_1(1.5)$ transition (~ 0.3).[26] The β value of ≈ 0.0 from the $P_1(1.5)$ transition is due to the fact that the $A^2\Sigma^+$ ($v' = 0$, $N' = 0$, $J' = 0.5$, F_1) final state has a rotational angular moment $N' = 0$ and thus an isotropic spatial distribution of the SH molecular axis prior to dissociation. The β values of the $Q_1(1.5)$ and $R_1(1.5)$ transitions depend on the initial alignments upon excitation and their subsequent reductions due to

depolarization during the excited-state lifetime that is longer than the molecular rotation period. The β parameters of the D(^{2}S) + S(^{3}P$_J$) products from the one-photon dissociation of SD A$^2\Sigma^+$ via the $P_1(1.5)$, $Q_1(1.5)$, and $R_1(1.5)$ transitions are similar to those of SH. The predissociation dynamics of the A$^2\Sigma^+$ ($v' = 0$, $N' = 0$-2, $J' = 0.5$-2.5) state of SH and SD have been studied and will be published in the future.[46, 47]

The two peaks at ~ 23000 and 10000 cm^{-1} in the $P(E_T)$ distributions of SH correlate with the peaks at ~ 16 and 24 μs in the H-atom TOF spectra. The high kinetic energies of these two product channels establish the involvement of two-photon excitation in the dissociation processes. The relative positions of the peaks around 23000 and 10000 cm^{-1} with respect to the three peaks from the H(^{2}S) + S(^{3}P$_J$) product channel in the $P(E_T,\theta)$ distributions are exactly consistent with the differences between the photon energy and the electronic energies of the S atom: S(^{1}D) at 9238.609 cm^{-1} and S(^{1}S) at 22179.954 cm^{-1} when S(^{3}P$_2$) at 0 cm^{-1}.[48] The two peaks at ~ 23000 and 10000 cm^{-1} are therefore assigned to the H(^{2}S) + S(^{1}D) and H(^{2}S) + S(^{1}S) products from the dissociation of the SH radical, respectively, following the two-photon excitations. The results for the SD A−X (0,0) transition are more complicated: in addition to the D(^{2}S) + S(^{3}P$_J$) products from predissociation of A$^2\Sigma^+$ via the one-photon (0,0) transition, the D(^{2}S) + S(^{1}D) and D(^{2}S) + S(^{1}S) products at ~ 23000 and 10000 cm^{-1} from the two-photon dissociation, there are products from other concurrent transitions. As displayed in Figure 4, in the $P(E_T,\theta)$ distributions of the D + S product from the photodissociation of the SD radical via the $P_1(1.5)$ transition, four signals at ~ 2500, 6000-7000, 8000-9000, ~ 10000 cm^{-1} (at the perpendicular photolysis polarization) remained when the photolysis wavelength is off the A$^2\Sigma^+$ (0,0) $P_1(1.5)$ resonance, which are assigned to the D(^{2}S) + S(^{1}D) products from photodissociation of SD (X$^2\Pi$, v'' = 6) via the repulsive wall of the A$^2\Sigma^+$ state, the D(^{2}S) + S(^{3}P$_J$) products from predissociation via the A$^2\Sigma^+$ (v'

= 5) (coincidently) excited from $X^2\Pi$ (v'' = 3), and the $D(^2S)$ + $S(^3P_J)$ products from direct dissociation of SD ($X^2\Pi$, v'' = 4 and 5) via the $^2\Sigma^-$ state, respectively. Although the signals from SD ($X^2\Pi$, v'' = 5) via the $^2\Sigma^-$ state overlap with the $D(^2S)$ + $S(^1S)$ product peak at ~ 10000 cm^{-1}, the latter dominates at the parallel polarization where the former is negligible due to the predominant perpendicular $^2\Sigma^- \leftarrow X^2\Pi$ transition.[42] The translational energy positions of the ~ 23000 and 10000 cm^{-1} peaks (the ~ 23 and 35 μs peaks in the TOF spectra) of SD also support the assignments of these two peaks to the $D(^2S)$ + $S(^1D)$ and $D(^2S)$ + $S(^1S)$ products from the two-photon dissociation of the SD radical, respectively.

Discussion

In Figure 3, the $H(^2S)$ + $S(^1D)$ peak at ~23000 cm^{-1} has a strong intensity at the perpendicular polarization and a much weaker signal at the parallel polarization, while the $H(^2S)$ + $S(^1S)$ peak around 10000 cm^{-1} is intense at the parallel polarization and negligible at the perpendicular polarization. During the two-photon dissociation, the first photon excites the SH radical to the $A^2\Sigma^+$ (v' = 0, N' = 0-2, J' = 0.5-2.5) state and partially aligns the axis of the SH radical, leading to an isotropic spatial distribution in N' = 0 following the $P_1(1.5)$ transition and slightly anisotropic distributions in N' = 1 and 2 following the $Q_1(1.5)$ and $R_1(1.5)$ transitions. Then the SH ($A^2\Sigma^+$) radical is sequentially excited by the second photon within the same 7-ns laser pulse to the higher states. In the sequential excitation, the second step can be considered as a one-photon process initiated from the partially aligned SH radical in the $A^2\Sigma^+$ (v' = 0, N' = 0-2, J' = 0.5-2.5) state. To estimate the β parameters of the second step in the two H + S dissociation channels, the

angular distributions via the $P_1(1.5)$ transition is used, in which the SH $A^2\Sigma^+$ ($v' = 0$, $N' = 0$, $J' = 0.5$) intermediate state is reached with an isotropic spatial distribution ($\beta \approx 0.0$ for the $H(^2S)$ + $S(^3P_J)$ products) and then the sequential second photon excitation is from a spatially *isotropic* distribution of SH in $A^2\Sigma^+$. For the two-photon dissociation via the $P_1(1.5)$ transition resonance, the β value for the $H(^2S)$ + $S(^1D)$ product is estimated to be $\sim -0.8 \pm 0.1$, indicating a predominantly perpendicular transition in the second-photon excitation for this product channel, while the $H(^2S)$ + $S(^1S)$ product channel has a β value of $\sim 1.3 \pm 0.3$, suggesting a dominant parallel transition in the second-photon excitation. The β values of the two-photon dissociation products $H(^2S)$ + $S(^1D)$ and $H(^2S)$ + $S(^1S)$ via the $Q_1(1.5)$ and $R_1(1.5)$ transitions are similar to those via the $P_1(1.5)$ transition. Among the possible spin-allowed doublet electronic excited states of SH, the states that can be energetically reached from the $A^2\Sigma^+$ state by the second photon excitation include $^2\Sigma^-$, $^2\Delta$, $2^2\Pi$, $B^2\Sigma^+$, and $2^2\Sigma^-$. Given that the one-photon $^2\Sigma^- \leftarrow A^2\Sigma^+$, $^2\Delta \leftarrow A^2\Sigma^+$ and $2^2\Sigma^- \leftarrow A^2\Sigma^+$ excitations are forbidden, the only allowed final states of SH accessed by the two-photon excitation in this work are $2^2\Pi$ and $B^2\Sigma^+$ (Figure 1). The bound-to-bound $2^2\Sigma^- \leftarrow A^2\Sigma^+$ transition is further ruled out, as the second photon is not on resonance of any rovibrational level of the $2^2\Sigma^-$ Rydberg state.[32] The $2^2\Pi \leftarrow A^2\Sigma^+$ excitation has a perpendicular transition dipole moment with respect to the S−H bond direction, while that of the $B^2\Sigma^+ \leftarrow A^2\Sigma^+$ transition is parallel to the S−H bond. During a prompt dissociation of the SH radical on a repulsive state, the nascent velocity of the H-atom should be along the S−H bond axis. The prompt dissociation on the repulsive $2^2\Pi$ state to the asymptotically correlated $H(^2S)$ + $S(^1D)$ products has a limit of $\beta = -1$, and the prompt dissociation of the $B^2\Sigma^+$ state asymptotically to $H(^2S)$ + $S(^1S)$ would result in a limiting β of 2. The observed anisotropy parameters in general agree with the repulsive PECs correlating to the different H + S product channels and that the $H(^2S)$ + $S(^1D)$ and $H(^2S)$ + $S(^1S)$ products are mainly from prompt

dissociations (in a very short time scale) on the repulsive $2^2\Pi$ and $B^2\Sigma^+$ states, respectively. The angle-integrated product translational energy distribution $P(E_T)$ can be derived from the $P(E_T,\theta)$ distributions at the perpendicular and parallel polarizations, which is used to obtain the branching ratios of different product channels. The branching ratio of the H(^{2}S) + S(^{1}D) and H(^{2}S) + S(^{1}S) product channels is estimated to be about 6.5 ± 2.5:1. As shown in Figure 1, the second photon reaches the energy region above the crossing point of the $2^2\Pi$ and $B^2\Sigma^+$ states, and the FC factor between the $A^2\Sigma^+$ ($v' = 0$) state and $B^2\Sigma^+$ is larger than with $2^2\Pi$. However, the H(^{2}S) + S(^{1}D) product channel (mainly from $2^2\Pi$) is observed to be more abundant than the H(^{2}S) + S(^{1}S) channel (mainly from $B^2\Sigma^+$). The major H(^{2}S) + S(^{1}D) products suggest that the transition dipole moment between $A^2\Sigma^+$ and $2^2\Pi$ is much larger than that between $A^2\Sigma^+$ and $B^2\Sigma^+$.

In the case of SD, the results from photodissociation via the A−X (0,0) transition are similar to that of SH. Figure 4 presents the data for the $P_1(1.5)$ transition, with the D(^{2}S) + S(^3P_J) products from the one-photon dissociation at ~ 1200 cm^{-1}. The D(^{2}S) + S(^{1}D) peak from the two-photon dissociation presents at ~23000 cm^{-1} with a stronger intensity at the perpendicular polarization. The β value for the D(^{2}S) + S(^{1}D) products is determined to be ~ −0.9 ± 0.05. The D(^{2}S) + S(^{1}S) signal from the two-photon dissociation locates around 10000 cm^{-1} at the parallel polarization, but at the perpendicular polarization there is a coincidental overlap with the D(^{2}S) + S(^3P_J) products from direct dissociation of SD ($X^2\Pi$, $v'' = 5$) via the $^2\Sigma^-$ state, with the S(^{1}S) peak locating between the S($^3P_1$) and S($^3P_2$) peaks. To determine the contributions from the overlapping signals, the peaks in the 9500-10500 cm^{-1} region in the perpendicular $P(E_T)$ distributions are initially deconvoluted to the D(^{2}S) + S(^3P_J) products with three slightly asymmetric double Gaussian peaks, with the relative positions of the three ^3P_J peaks fixed at the spin-orbit energy splitting of S(^3P_J) [S($^3P_2$): 0.0 cm^{-1}; S($^3P_1$), 396.1 cm^{-1}; S($^3P_0$), 573.6 cm^{-1}].[43] Based on the earlier experimental work on the

photodissociation following the $^2\Sigma^- – X^2\Pi$ excitation, the signals of the S(^3P_J) products in the $P(E_T)$ distributions are negligible at the parallel polarization and have a relative peak area ratio of S($^3P_{J=2,1,0}$) = 0.51:0.37:0.12 at the perpendicular polarization.[42] The S(^{1}S) peak from the two-photon dissociation at the perpendicular polarization is then deconvoluted after establishing its peak position from the parallel $P(E_T)$ distribution and the peak positions and intensities of the S(^3P_J) peaks. Subsequently, the β value for the D(^{2}S) + S(^{1}S) product channel is estimated to be ~ 1.2. The β values of the two-photon dissociation products D(^{2}S) + S(^{1}D) and D(^{2}S) + S(^{1}S) via the $Q_1(1.5)$ and $R_1(1.5)$ transitions are similar to those via the $P_1(1.5)$ transition. Similar to SH, the observed anisotropy parameters in SD agree with that the D(^{2}S) + S(^{1}D) and D(^{2}S) + S(^{1}S) products are primarily from prompt dissociations on the repulsive $2^2\Pi$ and $B^2\Sigma^+$ states, respectively. The branching ratio of the D(^{2}S) + S(^{1}D) and D(^{2}S) + S(^{1}S) product channels is estimated from the angle-integrated peak intensities to be about 5.7±1.7:1. Compared to SH, in SD the S(^{1}D) and S(^{1}S) two-photon signals are stronger relative to the S(^3P_J) one-photon signal, which is consistent with the much longer lifetime of SD $A^2\Sigma^+$ ($v' = 0, J' = 0.5$) (i.e., higher probability for the second-photon excitation).

The observed β parameters for both SH and SD do not reach the limit values. There are several possible origins: mixed transitions, depolarization due to an excited-state lifetime comparable to the rotational period, or a breakdown of the axial recoil approximation. For SH/SD in the studied energy region, mixed transitions are the most likely origin for the reduced β values. The SH/SD radical can be excited by the second photon from $A^2\Sigma^+$ to both the $2^2\Pi$ (a perpendicular transition) and $B^2\Sigma^+$ (a parallel transition) state. The $2^2\Pi$ and $B^2\Sigma^+$ state cross at a S-H distance of ~ 1.8 Å just outside of the FC region. The observation of reduced β parameters could be due to redistributions of some photofragment fluxes initiated on $2^2\Pi$ and $B^2\Sigma^+$ in the FC region via non-

adiabatic transitions at the crossing of the $2^2\Pi$ and $B^2\Sigma^+$ states. Due to the magnitude of the spin-orbit interaction in SH, the $2^2\Pi$ and $B^2\Sigma^+$ states could interact at their crossing point via spin-orbit coupling (e.g., through the Ω = ½ component), and the perpendicular and parallel dissociation fluxes initially from $2^2\Pi$ and $B^2\Sigma^+$ respectively in the FC region could redistribute and be mixed at the crossing point. The H(^{2}S) + S(^{1}D) product channel asymptotically on the $2^2\Pi$ PEC could then have some parallel component from $B^2\Sigma^+$, in addition to the main perpendicular contribution from $2^2\Pi$ in the FC region, and thus a reduced $\beta \sim -0.8$. Similarly, the H(^{2}S) + S(^{1}S) channel asymptotically on the $B^2\Sigma^+$ PEC could have some perpendicular component from $2^2\Pi$, in addition to the main parallel contribution from $B^2\Sigma^+$ in the FC region, and thus also a reduced $\beta \sim 1.3$. Specifically, the measured $\beta \sim -0.8 \pm 0.1$ for the H(^{2}S) + S(^{1}D) channel indicates that the percentages of the parallel and perpendicular characters are $7 \pm 3\%$:$93 \pm 3\%$, while the $\beta \sim 1.3 \pm 0.3$ for the H(^{2}S) + S(^{1}S) channel results from a $77 \pm 10\%$:$23 \pm 10\%$ mix of the parallel and perpendicular components.[45, 49] Similarly for SD, the measured $\beta \sim -0.9 \pm 0.05$ for D(^{2}S) + S(^{1}D) implies percentages of the parallel and perpendicular characters of $\sim 3 \pm 2\%$:$97 \pm 2\%$; while the $\beta \sim 1.2$ for D(^{2}S) + S(^{1}S) is from a ~ 73%:27% mix of the parallel and perpendicular components.[45, 49] In order to study the photodissociation flux redistributions behind the reduced β values, it is important to characterize the nonadiabatic transitions at the crossing of $2^2\Pi$ and $B^2\Sigma^+$.

Based on the Landau–Zener model,[50] the nonadiabatic transition probability P between two diabatic potential curves at the crossing can be described as $P = 1 - \exp\left[-\frac{2\pi V_{ab}^2}{\hbar v|F_a - F_b|}\right]$, where V_{ab} is the coupling between diabatic potential curves of the a and b states, v is the velocity of particles involved in the crossing, and F_a and F_b are the slope of the diabatic curve a and b at the crossing. All the parameters above can be estimated from the calculated PECs in Figure 1, except that there is no available value for the spin-orbit coupling V_{ab} between $2^2\Pi$ and $B^2\Sigma^+$. To illustrate the

photodissociation flux redistributions and mechanism, it is possible to estimate the spin-orbit coupling V_{ab} and transition probability P by simulating and optimizing the β values in comparison with their experimental values. By starting with the (trial) probability ratio of initial photoexcitation to the $2^2\Pi$ state (sum of perpendicular components) and to the $B^2\Sigma^+$ state (sum of parallel components) in the FC region and the subsequent non-adiabatic transition probability P (which depends on the (trial) V_{ab} value) between $2^2\Pi$ and $B^2\Sigma^+$ at the crossing point, the final product branching ratio of S(^{1}D)/S(^{1}S) and the mix of parallel and perpendicular components (thus the β value) of both the H(^{2}S) + S(^{1}D) and H(^{2}S) + S(^{1}S) product channels can be modeled and compared with the experimental branching ratio (~ 6.5:1) and β values. When the modeled S(^{1}D)/S(^{1}S) product branching ratio is the same as the experimental value (6.5:1), the β value predictions closest to the experimental measurements of SH are: $\beta = -0.98$ for H(^{2}S) + S(^{1}D) and $\beta = 1.3$ for H(^{2}S) + S(^{1}S), with the spin-orbit coupling V_{ab} ~ 60-65 cm^{-1} and the transition probability P ~ 3-4% for SH. The estimated spin-orbit coupling V_{ab} between $2^2\Pi$ and $B^2\Sigma^+$ is in the range of those of other excited states of SH (such as between $A^2\Sigma^+$ and $^4\Sigma^-$, $^2\Sigma^-$, and $^4\Pi$).[4] The modeling for the β of the H(^{2}S) + S(^{1}S) products is in a good agreement with the experiment, while that for the H(^{2}S) + S(^{1}D) products is relatively poor. Nevertheless, this modeling using the Landau-Zener model provides qualitatively insight into the nonadiabatic coupling and dissociation mechanisms of the SH $2^2\Pi$ and $B^2\Sigma^+$ states. For SD, by using the experimental product ratio of S(^{1}D)/S(^{1}S) (~ 5.7:1) and the experimental β values of the D(^{2}S) + S(^{1}D) and D(^{2}S) + S(^{1}S) products, the nonadiabatic transition probability P can be modelled to be ~ 4-5% with the same spin-orbit coupling V_{ab} of ~ 60-65 cm^{-1} as in SH. This P value in SD is larger than that for SH and is consistent with the slower dissociation velocity of the D atom. The modeled S(^{1}D)/S(^{1}S) product branching ratio in SD is the same as the experimental value (5.7:1). The agreement between the

prediction of β parameters and the experiment ones in SD is better than in SH, in which the calculated $\beta = -0.98$ for D(^{2}S) + S(^{1}D) and $\beta = 1.2$ for D(^{2}S) + S(^{1}S)) based on the Landau–Zener model.

Note that in a similar two-photon dissociation of OH via its $A^2\Sigma^+$ state, the second photon also excites $A^2\Sigma^+$ to both the $2^2\Pi$ (a perpendicular transition) and $B^2\Sigma^+$ (a parallel transition) state. The $\beta = -0.97$ for H(^{2}S) + O(^{1}D) via the $2^2\Pi$ PEC and $\beta = 1.97$ for H(^{2}S) + O(^{1}S) via the $B^2\Sigma^+$ PEC, near the limit value of a parallel and perpendicular transition, respectively.[44] When applying the Landau–Zener model along with the product ratio O(^{1}D)/O(^{1}S) $\approx$ 3:4,[44] the best predictions are obtained as $\beta = -0.96$ for H(^{2}S) + O(^{1}D) and $\beta = 1.98$ for H(^{2}S) + O(^{1}S), and the spin-orbit coupling between the $2^2\Pi$ and $B^2\Sigma^+$ states of OH is estimated to be 20 cm^{-1} (with $P\sim$ 1%). This indicates that the dissociation fluxes from the $2^2\Pi$ and $B^2\Sigma^+$ states in OH almost do not mix, consistent with the much smaller spin-orbit coupling in OH than in SH/SD.[51] The agreement between the modeling and experimental β values for OH is better than for SH/SD. In the case of SH/SD, the deviation might result from the uncertainties in experimental measurements, and furthermore there are several estimations in the Landau–Zener calculations in the current study, e.g. the crossing position between $2^2\Pi$ and $B^2\Sigma^+$ and the values of the diabatic force F_a and F_b of the two PECs. Overall, the product angular distributions indicate that upon the sequential two-photon excitation the SH/SD $2^2\Pi$ and $B^2\Sigma^+$ states undergo repulsive, prompt dissociations, along with a small amount of non-adiabatic crossings and redistributions of photodissociation flux between them, leading to the H/D(^{2}S) + S(^{1}D) and H/D(^{2}S) + S(^{1}S) products, respectively. And the Landau-Zener model calculations qualitatively support the nonadiabatic coupling and dissociation mechanisms of the SH/SD $2^2\Pi$ and $B^2\Sigma^+$ states.

With conservation of energy and the electronic energies of the S atom and H atom,

$$E_{hv} + E_{\text{int}}(\text{SH}) - D_0(\text{S}-\text{H}) = E_{\text{T}} + E_{\text{elec}}(\text{S}) = \frac{1}{2}m_{\text{H}}(1 + \frac{m_{\text{H}}}{m_{\text{S}}})(\frac{L}{t_{\text{H}}})^2 + \frac{m_{\text{H}}}{m_{\text{S}}}E_{\text{SH}} + E_{\text{elec}}(\text{S}) \quad (3)$$

where E_{hv} is the photon(s) energy, $E_{\text{int}}(\text{SH})$ is the initial internal energy of SH radical, $D_0(\text{S}-\text{H})$ is the bond dissociation energy of ground-state SH ($X^2\Pi$, $v'' = 0$, $N'' = 1$, $J'' = 1.5$, F_1), and $E_{\text{elec}}(\text{S})$ is the electronic energy of the S-atom product. Since the $P_1(1.5)$, $Q_1(1.5)$, and $R_1(1.5)$ transitions are all excited from the same SH ground state, $E_{\text{int}}(\text{SH}) = 0$, the equation (3) can be rewritten as

$$E_{hv} - E_{\text{elec}}(\text{S}) = \frac{1}{2}m_{\text{H}}(1 + \frac{m_{\text{H}}}{m_{\text{S}}})(\frac{L}{t_{\text{H}}})^2 + \frac{m_{\text{H}}}{m_{\text{S}}}E_{\text{SH}} + D_0(\text{S}-\text{H}) \quad (4)$$

By building a linear regression of $E_{hv} - E_{\text{elec}}(\text{S})$ versus $(1/t_H)^2$, using the TOF peak positions of the two-photon products $H(^2S) + S(^1D)$ and $H(^2S) + S(^1S)$ and the one-photon product $H(^2S) + S(^3P_2)$ from $A^2\Sigma^+$ ($v' = 0$-2, $J' = 0.5$-2.5) (for $v' = 1$ and 2 only the relatively pure $Q_1(1.5)$ results are used, which are from our another work[46, 47]), and the well-known electronic energy levels of the S atom, the *y*-intercept gives $D_0(\text{S}-\text{H}) + (m_{\text{H}}/m_{\text{S}})E_{\text{SH}}$, and the refined calibration of L can be determined from the slope. About 25 TOF peak positions are included in the linear regression to achieve a high precision. As $(m_{\text{H}}/m_{\text{S}})E_{\text{SH}}$ is determined to be ~ 14 cm^{-1}, an accurate S−H bond dissociation energy of $D_0(\text{S}-\text{H}) = 29253 \pm 20$ cm^{-1} is obtained. This experimental value is consistent with a previous experimental measurement of 29300 ± 100 cm^{-1} by Ashfold and co-workers,[38, 39] and it is in a good agreement with the theoretical values: 29234^{+42}_{-37} cm^{-1} derived from extensive high-level ab initio electronic structure calculations,[52] 20249 ± 170 cm^{-1} at the CCSD(T)/aug-ccpV6Z level of theory by Peebles and Marshall,[53] and 29249 cm^{-1} based on the G3 theory by Curtiss et al.[54] In the case of SD, $(m_{\text{D}}/m_{\text{S}})E_{\text{SD}}$ is about 29 cm^{-1}, and the bond dissociation energy is determined similarly to be $D_0(\text{S}-\text{D}) = 29650 \pm 20$ cm^{-1}. Our value agrees with the previous measurement of 29700 ± 100 cm^{-1} by Ashfold and co-workers.[38, 39] Compared

to our previous experimental results: D_0(S−H) = 29245 ± 25 cm^{-1},[40] and D_0(S−D) = 29660 ± 25 cm^{-1},[42] the newly determined values in this work improve with reduced uncertainty.

With the derived bond dissociation energy of the ground state $D_0(\mathrm{X}^2\Pi)$, the dissociation energy of the $\mathrm{A}^2\Sigma^+$ state can be determined as well. To determine $D_0(\mathrm{A}^2\Sigma^+)$ (from the zero-point of the $\mathrm{A}^2\Sigma^+$ state), the equality of energy is used:

$$T_{00} + D_0(\mathrm{A}^2\Sigma^+) = D_0(\mathrm{X}^2\Pi) + E\left[S(^1D)\right] - E\left[S(^3P_2)\right] \quad (5)$$

where T_{00} is the excitation energy of the $\mathrm{A}^2\Sigma^+$ ($v' = 0$, $N' = 0$, $J' = 0.5$, F_1) ← $\mathrm{X}^2\Pi$ ($v'' = 0$, $N'' = 1$, $J'' = 1.5$, F_1) transition from earlier experimental studies, i.e. 30832.68 cm^{-1} for SH and 30948.24 cm^{-1} for SD;[9] and $E\left[S(^1D)\right] - E\left[S(^3P_2)\right]$ is the well-known energy separation of the $^3P_2$ ground and ^1D excited state of atomic sulfur (9238.609 cm^{-1}).[48] With the presently determined values of $D_0(\mathrm{X}^2\Pi)$, the $D_0(\mathrm{SH}, \mathrm{A}^2\Sigma^+)$ is derived to be 7659 ± 20 cm^{-1}, and $D_0(\mathrm{SD}, \mathrm{A}^2\Sigma^+)$ = 7940 ± 20 cm^{-1}. In the previously experimental studies, Johns and Ramsay proposed the value of D_0 $(\mathrm{SH}, \mathrm{A}^2\Sigma^+)$ = 8020 ± 1000 cm^{-1} based on a linear extrapolation of the $\mathrm{A}^2\Sigma^+$ v' = 0-2 vibrational energies followed by an empirical correction.[10] With the detected rovibrational terms of the SH $\mathrm{A}^2\Sigma^+$ state (v' = 0-4), Schnieder et al. obtained the best-fit potential and determined $D_0(\mathrm{SH}, \mathrm{A}^2\Sigma^+)$ = 8320 ± 600 cm^{-1}.[14] Western and co-workers redetermined $D_0(\mathrm{A}^2\Sigma^+)$ to be 7705 ± 100 cm^{-1} for SH and 7974 ± 100 cm^{-1} for SD, using the T_{00} and the zero-point energy derived by Ramsay.[38] Clearly, our dissociation energies of the SH and SD $\mathrm{A}^2\Sigma^+$ state agree with the earlier experimental values within the experimental uncertainties and are of higher accuracy. Our experimental D_0 $(\mathrm{A}^2\Sigma^+)$ values are substantially larger than those suggested by all existing ab initio calculations of the SH $\mathrm{A}^2\Sigma^+$ state: $D_0(\mathrm{A}^2\Sigma^+)$ = 4686 cm^{-1},[1] 4358 cm^{-1},[2] 6809 cm^{-1},[5] 6856 cm^{-1},[6] and 6311 cm^{-1}.[8]

Conclusion

The photodissociation of the SH/SD radical is studied via the $P_1(1.5)$, $Q_1(1.5)$, and $R_1(1.5)$ transition resonances ($A^2\Sigma^+$ ($v' = 0$, $N' = 0$-2, $J' = 0.5$-2.5, F_1/F_2) ← $X^2\Pi$ ($v'' = 0$, $N'' = 1$, $J'' = 1.5$, F_1)). The H/D(^{2}S) + S(^{1}D) and H/D(^{2}S) + S(^{1}S) product channels are observed and result primarily from the dissociation of the SH/SD radical on the $2^2\Pi$ and $B^2\Sigma^+$ states, respectively, following sequential two-photon excitations via the $A^2\Sigma^+$ intermediate state. These two product channels have anisotropic angular distributions, with $\beta \approx -0.8 \pm 0.1$ for H(^{2}S) + S(^{1}D) (-0.9 ± 0.05 for SD) and $\beta \approx 1.3 \pm 0.3$ for H(^{2}S) + S(^{1}S) (1.2 for SD). The branching ratio of the H(^{2}S) + S(^{1}D) to H(^{2}S) + S(^{1}S) channel is estimated to be $\sim 6.5 \pm 2.5$:1 ($\sim 5.7 \pm 1.7$:1 in the case of SD). The dynamics of these electronic excited S-atom product channels would be prompt dissociation of the SH/SD radical on the repulsive $2^2\Pi$ and $B^2\Sigma^+$ states with a small amount of non-adiabatic crossings and redistributions of photodissociation flux between them, leading to the H/D(^{2}S) + S(^{1}D) and H/D(^{2}S) + S(^{1}S) product channel, respectively. The bond dissociation energy of SH is determined to be D_0(S−H) = 29253±20 cm^{-1}, and D_0(S−D) = 29650±20 cm^{-1} for SD. The dissociation energy of the $A^2\Sigma^+$ state is also obtained: D_0[S−H(A)] = 7659 ± 20 cm^{-1} and D_0[S−D(A)] = 7940 ± 20 cm^{-1}.

Acknowledgement

This work was supported by the US National Science Foundation (grant number CHE-1566636 and CHE-2155232).

References

1. D. M. Hirst and M. F. Guest, *Mol. Phys.*, 1982, **46**, 427-435.
2. P. J. Bruna and G. Hirsch, *Mol. Phys.*, 1987, **61**, 1359-1380.
3. J. K. Park and H. Sun, *Chem. Phys. Lett.*, 1992, **194**, 485-491.
4. M. R. Manaa, *Int. J. Quantum Chem., Quantum Chem. Symp*, 1995, **56**, 577-584.
5. S. M. Resende and F. R. Ornellas, *J. Chem. Phys.*, 2001, **115**, 2178-2187.
6. V. Brites, D. Hammoutène and M. Hochlaf, *J. Phys. B: At. Mol. Opt. Phys.*, 2008, **41**, 045101.
7. B. S. D. R. Vamhindi and M. Nsangou, *Mol. Phys.*, 2016, **114**, 2204-2216.
8. S.-T. Zhao, X.-P. Liu, R. Li, H.-J. Guo and B. Yan, *Chin. Phys. B*, 2021, **30**, 073104.
9. D. A. Ramsay, *J. Chem. Phys.*, 1952, **20**, 1920-1927.
10. J. W. C. Johns and D. A. Ramsay, *Can. J. Phys.*, 1961, **39**, 210-217.
11. W. Ubachs, J. J. ter Meulen and A. Dymanus, *Chem. Phys. Lett.*, 1983, **101**, 1-5.
12. R. R. Friedl, W. H. Brune and J. G. Anderson, *J. Chem. Phys.*, 1983, **79**, 4227-4236.
13. J. J. Tiee, M. J. Ferris and F. B. Wampler, *J. Chem. Phys.*, 1983, **79**, 130-133.
14. L. Schnieder, W. Meier, K. H. Welge, M. N. R. Ashfold and C. M. Western, *J. Chem. Phys.*, 1990, **92**, 7027-7037.
15. S. H. Ashworth and J. M. Brown, *J. Mol. Spectrosc.*, 1992, **153**, 41-58.
16. E. Klisch, T. Klaus, S. P. Belov, A. Dolgner, R. Schieder, G. Winnewisser and E. Herbst, *Astrophys. J.*, 1996, **473**, 1118.
17. M. D. Wheeler, A. J. Orr-Ewing and M. N. R. Ashfold, *J. Chem. Phys.*, 1997, **107**, 7591-7600.
18. M. N. Lewis and J. U. White, *Phys. Rev.*, 1939, **55**, 894-898.

19. C. M. Pathak and H. B. Palmer, *J. Mol. Spectrosc.*, 1969, **32**, 157-162.

20. K. H. Becker and D. Haaks, *J. Photochem.*, 1972, **1**, 177-179.

21. J. Senekowitsch, H. J. Werner, P. Rosmus, E. A. Reinsch and S. V. ONeil, *J. Chem. Phys.*, 1985, **83**, 4661-4667.

22. D. Zeitz, W. Bohle, J. Werner, A. Hinz and W. Urban, *Mol. Phys.*, 1985, **54**, 953-958.

23. G. W. Loge and J. J. Tiee, *J. Chem. Phys.*, 1988, **89**, 7167-7171.

24. M. Kawasaki, H. Sato, G. Inoue and M. Suzuki, *J. Chem. Phys.*, 1989, **91**, 6758-6764.

25. M. D. Wheeler, A. J. Orr-Ewing, M. N. R. Ashfold and T. Ishiwata, *Chem. Phys. Lett.*, 1997, **268**, 421-428.

26. R. A. Rose, A. J. Orr-Ewing, C.-H. Yang, K. Vidma, G. C. Groenenboom and D. H. Parker, *J. Chem. Phys.*, 2009, **130**, 034307.

27. M. N. Gorman, S. N. Yurchenko and J. Tennyson, *Mon. Not. R. Astron. Soc.*, 2019, **490**, 1652-1665.

28. A. Fast and S. A. Meek, *J. Chem. Phys.*, 2021, **154**, 114304.

29. S. Lee and H. Seon, *Bull. Korean Chem. Soc.*, 2001, **22**, 210-212.

30. S. Lee, H. Sun, B. Kim and K. F. Freed, *J. Chem. Phys.*, 2001, **114**, 5537-5544.

31. L. M. C. Janssen, M. P. J. van Der Loo, G. C. Groenenboom, S.-M. Wu, D. Č. Radenović, A. J. van Roij, I. A. Garcia and D. H. Parker, *J. Chem. Phys.*, 2007, **126**, 094304.

32. B. A. Morrow, *Can. J. Phys.*, 1966, **44**, 2447-2459.

33. M. N. R. Ashfold, B. Tutcher and C. M. Western, *Mol. Phys.*, 1989, **66**, 981-991.

34. J. B. Milan, W. J. Buma, C. A. de Lange, C. M. Western and M. N. R. Ashfold, *Chem. Phys. Lett.*, 1995, **239**, 326-331.

35. J. B. Milan, W. J. Buma and C. A. De Lange, *J. Chem. Phys.*, 1996, **105**, 6688-6712.

36. R. E. Continetti, B. A. Balko and Y. T. Lee, *Chem. Phys. Lett.*, 1991, **182**, 400-405.

37. C.-W. Hsu, C.-L. Liao, Z.-X. Ma, P. J. H. Tjossem and C. Y. Ng, *Chem. Phys. Lett.*, 1992, **199**, 78-84.

38. G. P. Morley, I. R. Lambert, D. H. Mordaunt, S. H. S. Wilson, M. N. R. Ashfold, R. N. Dixon and C. M. Western, *J. Chem. Soc., Faraday trans.*, 1993, **89**, 3865-3876.

39. S. H. S. Wilson, J. D. Howe and M. N. R. Ashfold, *Mol. Phys.*, 1996, **88**, 841-858.

40. W. Zhou, Y. Yuan, S. Chen and J. Zhang, *J. Chem. Phys.*, 2005, **123**, 054330.

41. S. Chen, W. Zhou and J. Zhang, *Chem. Phys. Lett.*, 2006, **418**, 328-332.

42. X. Zheng, J. Wu, Y. Song and J. Zhang, *Phys. Chem. Chem. Phys.*, 2009, **11**, 4761-4769.

43. G. Sun, W. Zhou, X. Zheng, Y. Qin, Y. Song, Y. Yuan and J. Zhang, *Mol. Phys.*, 2021, **119**, e1837974.

44. G. Sun, X. Zheng, Y. Qin, Y. Song, J. Zhang, J. M. Amero and G. J. Vázquez, *Chin. J. Chem. Phys.*, 2020, **33**, 129-134.

45. R. N. Zare, *Mol. Photochem.*, 1972, **4**, 1-37.

46. Y. Qin, X. Zheng, Y. Song, G. Sun and J. Zhang, unpublished work.

47. Y. Qin, X. Zheng, Y. Song, G. Sun and J. Zhang, unpublished work.

48. A. Kramida, Yu. Ralchenko, J. Reader, and NIST ASD Team (2021), NIST Atomic Spectra Database (ver. 5.9) [Online], https://physics.nist.gov/asd (accessed 2022 June 16).

49. G. N. A. van Veen, K. A. Mohamed, T. Baller and A. E. De Vries, *Chem. Phys.*, 1983, **80**, 113-120.

50. E. E. Nikitin, in *Theory of elementary atomic and molecular processes in gases*, Clarendon Press, Oxford, 1974, ch. 3.

51. G. Parlant and D. R. Yarkony, *J. Chem. Phys.*, 1999, **110**, 363-376.

52. A. G. Csaszar, M. L. Leininger and A. Burcat, *J. Phys. Chem. A*, 2003, **107**, 2061-2065.

53. L. R. Peebles and P. Marshall, *J. Chem. Phys.*, 2002, **117**, 3132-3138.

54. L. A. Curtiss, K. Raghavachari, P. C. Redfern, V. Rassolov and J. A. Pople, *J. Chem. Phys.*, 1998, **109**, 7764-7776.

Figures and Captions

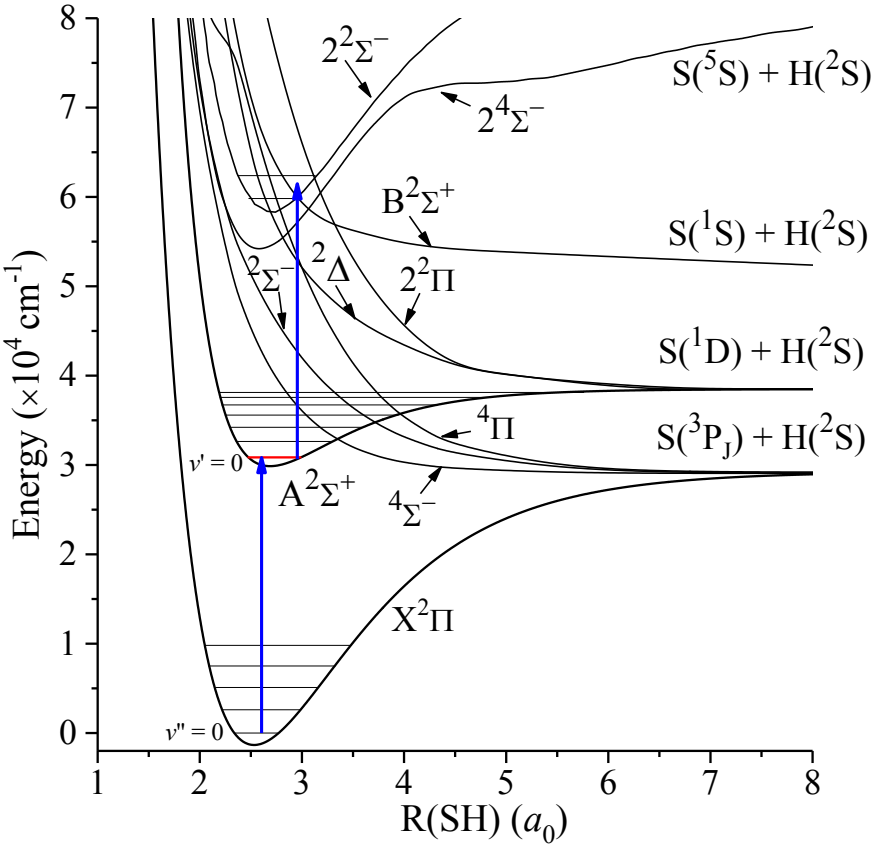

Figure 1 Potential energy curves of the SH system. The vibrational levels $v'' = 0$-4 of the $X^2\Pi$ state, $v' = 0$-6 of the $A^2\Sigma^+$ state, and $v = 0$-1 of the $2^2\Sigma^-$ state are shown. The information is from Refs. 3-5, 8.

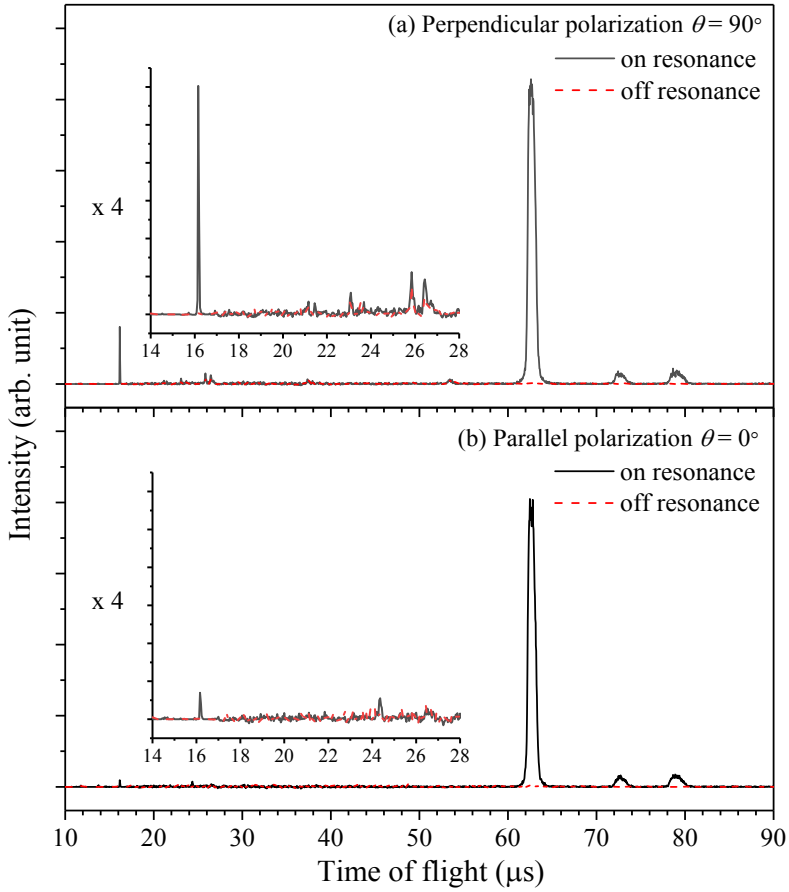

Figure 2 H-atom TOF spectra of the photodissociation of the SH radical via the $A^2\Sigma^+$ ($v' = 0$, $N' = 0$, $J' = 0.5$, F_1) ← $X^2\Pi$ ($v'' = 0$, $N'' = 1$, $J'' = 1.5$, F_1) transition (the $P_1(1.5)$ transition), with the polarization of the photolysis radiation (a) perpendicular and (b) parallel to the TOF path. The spectra are scaled to the same number of photolysis laser shots and laser power.

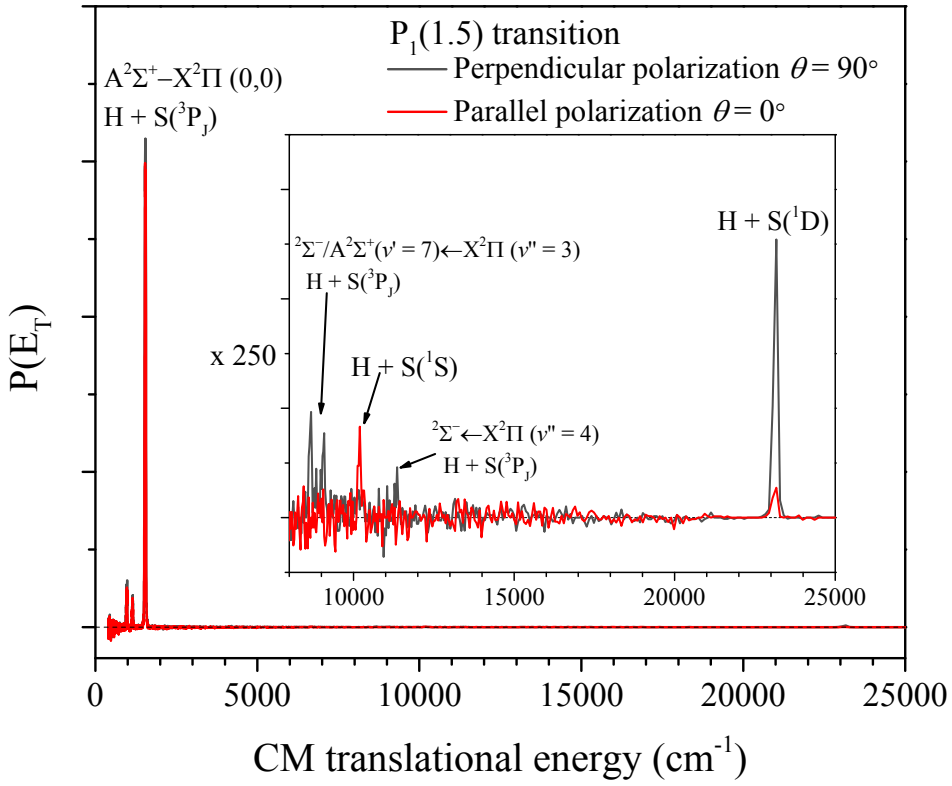

Figure 3 Center-of-mass product channel translational energy distribution from the photodissociation of SH via the $A^2\Sigma^+$ ($v' = 0$, $N' = 0$, $J' = 0.5$, F_1) ← $X^2\Pi$ ($v'' = 0$, $N'' = 1$, $J'' = 1.5$, F_1) transition $P_1(1.5)$, with the linearly polarized photolysis radiation perpendicular (black curve) and parallel (red curve) to the TOF axis. The inset in the figure depicts an enlarged region in the 7500 to 25000 cm^{-1} product translational energy. Different S-atom product channels are indicated in the figure. See the text for more details.

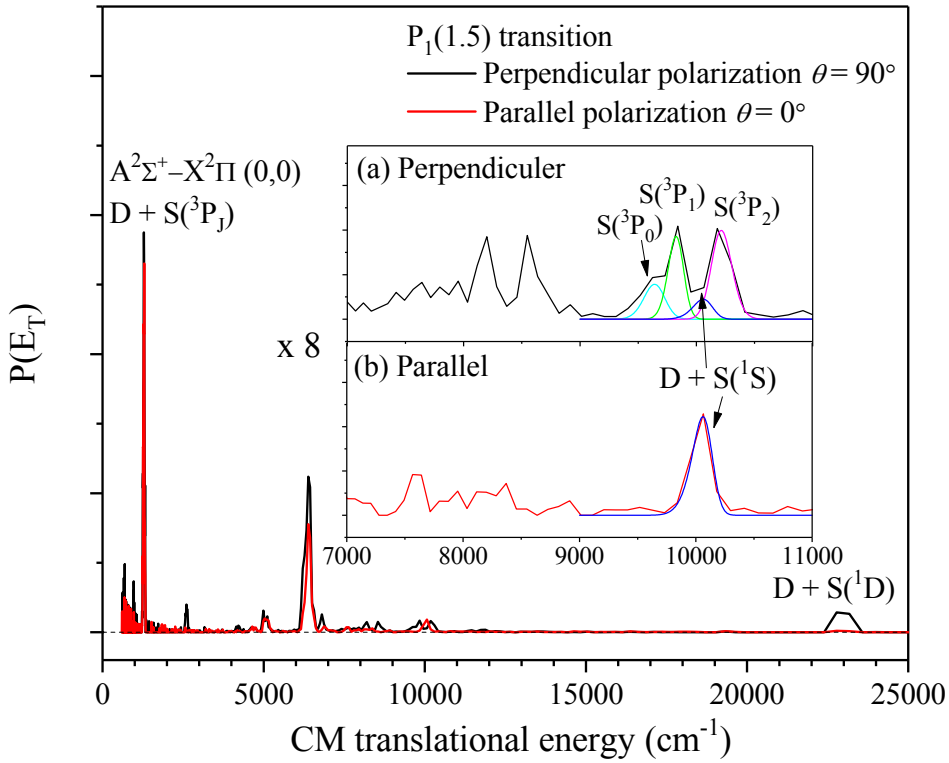

Figure 4 Center-of-mass product channel translational energy distribution from the photodissociation of SD via the $A^2\Sigma^+$ ($v' = 0$, $N' = 0$, $J' = 0.5$, F_1) ← $X^2\Pi$ ($v'' = 0$, $N'' = 1$, $J'' = 1.5$, F_1) transition $P_1(1.5)$, with the linearly polarized photolysis radiation perpendicular (black curve) and parallel (red curve) to the TOF axis. The inset in the figure depicts an enlarged region in the 7000 to 11000 cm^{-1} product translational energy. Different S-atom product channels are present in the figure: in addition to the $D(^2S) + S(^1D)$ and $D(^2S) + S(^1S)$ products from the two-photon excitation, there are the $D(^2S) + S(^3P_J)$ products from $A^2\Sigma^+$ ($v' = 0$) ← $X^2\Pi$ ($v'' = 0$) at 700-1300 cm^{-1}, $A^2\Sigma^+$ ($v' = 3$) ← $X^2\Pi$ ($v'' = 2$) at ~5000 cm^{-1}, $A^2\Sigma^+$ ($v' = 5$) ← $X^2\Pi$ ($v'' = 3$) at 6000-7000 cm^{-1}, $^2\Sigma^-$ ← $X^2\Pi$ ($v'' = 4$) at 8000-9000 cm^{-1}, and $^2\Sigma^-$ ← $X^2\Pi$ ($v'' = 5$) at 9500-10500 cm^{-1}; and the $D(^2S) + S(^1D)$ products from the repulsive wall of the $A^2\Sigma^+$ ← $X^2\Pi$ ($v'' = 6$) at ~2600 cm^{-1}. In the energy region of 9000-11000 cm^{-1}, the $D(^2S) + S(^3P_J)$ products from $^2\Sigma^-$ ← $X^2\Pi$ ($v'' = 5$) and the $D(^2S) + S(^1S)$ peak from the two-photon dissociation are deconvoluted by fitting with slightly asymmetric Gaussian peaks and are shown in the inset: cyan curve for $S(^3P_0)$, green curve for $S(^3P_1)$, magenta curve for $S(^3P_2)$, and blue curve for $S(^1S)$. See the text for more details.